Hindawi Publishing Corporation
International Journal of Optics
Volume 2015, Article ID 815967, 7 pages
http://dx.doi.org/10.1155/2015/815967

Research Article

Investigation on the Effect of Underwater Acoustic Pressure on the Fundamental Mode of Hollow-Core Photonic Bandgap Fibers

Adel Abdallah, Zhang Chaozhu, and Zhong Zhi

College of Information and Communication Engineering, Harbin Engineering University, Nantong Street 145, Nantong, Harbin, Heilongjiang 150001, China

Correspondence should be addressed to Adel Abdallah; adelmtc39@gmail.com

Received 16 December 2014; Accepted 16 March 2015

Academic Editor: Alejandro Aceves

Recently, microstructured optical fibers have become the subject of extensive research as they can be employed in many civilian and military applications. One of the recent areas of research is to enhance the normalized responsivity (NR) to acoustic pressure of the optical fiber hydrophones by replacing the conventional single mode fibers (SMFs) with hollow-core photonic bandgap fibers (HC-PBFs). However, this needs further investigation. In order to fully understand the feasibility of using HC-PBFs as acoustic pressure sensors and in underwater communication systems, it is important to study their modal properties in this environment. In this paper, the finite element solver (FES) COMSOL Multiphysics is used to study the effect of underwater acoustic pressure on the effective refractive index (n_{eff}) of the fundamental mode and discuss its contribution to NR. Besides, we investigate, for the first time to our knowledge, the effect of underwater acoustic pressure on the effective area (A_{eff}) and the numerical aperture (NA) of the HC-PBF.

1. Introduction

Optical fiber hydrophone is a significant area of research. For many years, researchers have shown the prospects of using the conventional SMF interferometric hydrophones as alternatives to the conventional sound navigation and ranging (SONAR) systems [1]. However, the conventional SMF is made of glass that has high Young's modulus (E); in addition, its change of effective refractive index of the fundamental mode (n_{eff}) due to applied acoustic pressure has opposite sign with respect to length change, and hence both affect NR [2]. As a result, researchers began to search for alternatives to enhance NR. One possible solution is to test the microstructured optical fibers that can be classified into two classes: solid-core PCF (SC-PCF) and HC-PBF. It was shown experimentally that SC-PCF has about the same phase sensitivity to axial strain as SMF [3]. As a result, using SC-PCF as alternatives to SMF is infeasible. However, because SC-PCFs are bend-insensitive, they can be used to reduce the hydrophone size [4]. It was reported that HC-PBFs have many advantages over SMFs that provide better responsivity to measurands and eligibility for many sensing applications [2, 5–7]. Some of these advantages are as follows. (1) The design and manufacturing flexibility of HC-PBFs reduces the effective Young's modulus of the fiber and enhances the NR of the HC-PBF to acoustic pressure [2], (2) matching between the mode indexes of the HC-PBF with the ambient air helps to reduce the back-reflected light at the fiber end faces which is useful for many applications [7], (3) holes of the HC-PBF can be filled with a substance with opposite thermal expansion to make the material insensitive to temperature [5], (4) in the HC-PBF, because the optical mode propagates in air, it has smaller Faraday, Kerr, and thermal constants than solid-silica cores, and this reduces the dependencies on temperature, magnetic field, and power fluctuations [5], and (5) HC-PBFs are almost entirely bend-insensitive and can be bent to very small diameters (<1 cm) with minimal loss, and this makes it suitable for small-size hydrophone systems [6, 8]. However, using HC-PBFs as underwater acoustic sensors needs further investigation to be feasible alternatives to their

counterparts of SMFs. Effective mode area (A_{eff}) is a key factor in designing PCFs [9]. It determines how tightly the mode is confined to the core of the fiber. The effective area can be used to study the nonlinearities, mode-field diameter (MFD), confinement losses, bending losses, splicing losses, and numerical aperture (NA) of the optical fiber [9, 10]. For this reason, studying the effect of acoustic pressure on A_{eff} allows getting information and important relations about how the acoustic pressure affects other important quantities. For accurate results, it is important to accurately model A_{eff} of the HC-PBF. It was proposed in [11] that the electrical field distribution of the PCFs is non-Gaussian and cannot be determined by assuming a conventional step-index distribution. Also, it was found that the ITU-T Petermann II definition is the most suitable for describing A_{eff} and MFD of PCFs with non-Gaussian distribution; as a result, it is adopted in this paper. ITU-T stands for the International Telecommunication Union-Telecommunication Standardization Sector [12]. To our knowledge, the effect of underwater acoustic pressure on A_{eff} of HC-PBF has not been studied. In this paper, we study the interferometric optical fiber hydrophone, which is based on acoustic pressure to phase transduction mechanism, in which the investigated HC-PBF represents its measuring arm. The effect of underwater acoustic pressure on the fundamental mode of hollow-core photonic bandgap fibers is investigated by coupling between the acoustic-solid interaction (ASI) and the electromagnetic waves (EMW) modules in the FES COMSOL Multiphysics. The ASI module is used to apply acoustic pressures of different amplitudes and frequencies that cause structural deformation and the induced stresses and strains for the investigated HC-PBF are calculated. The EMW module in the FES is used to calculate n_{eff} for undeformed HC-PBF; then the coupled ASI and EMW modules are used to calculate n_{eff} for the deformed fiber. This enables us to study and analyse the effect of acoustic pressure on n_{eff}, A_{eff}, the MFD, and NA of the investigated HC-PBF. The investigated HC-PBF is the commercial HC-1550 with air-filling ratio (η) of 92% that represents the ratio of the air hole diameter (d_h) in the microstructured cladding to the pitch (Λ) which is the central distance between two adjacent air holes. The used parameters of the investigated fiber are listed in Table 1.

Table 1: Physical parameters of the investigated optical fiber [2, 6].

Region	HC-PBF
Core	Material: air $d_1 = 10.1\,\mu$m
Clad	Air-silica honeycomb $d_2 = 70\,\mu$m, $\nu_2 = 0.17$, $\Lambda = 3.8\,\mu$m $d_h = 3.5\,\mu$m, $\eta = 92\%$ $E_r = E_\theta = (3/2)(1-\eta)^3 E_o$ $E_z = (1-\eta)\,E_o$ Solid-silica clad $d_3 = 120\,\mu$m, $E_3 = 72$ GPa, $\nu_3 = 0.17$
Polymer coating	Material: acrylate $t = 93.5\,\mu$m, $E_4 = 0.75$ GPa, $\nu_4 = 0.45$

E is Young's modulus of each layer, E_o is Young's modulus of the silica, ν is Poisson's ratio, d is the diameter of each region, d_h is the air hole diameter in the microstructured region, t is the thickness of the acrylate coating, and E_r, E_θ, and E_z are used to describe the anisotropy of the microstructured area.

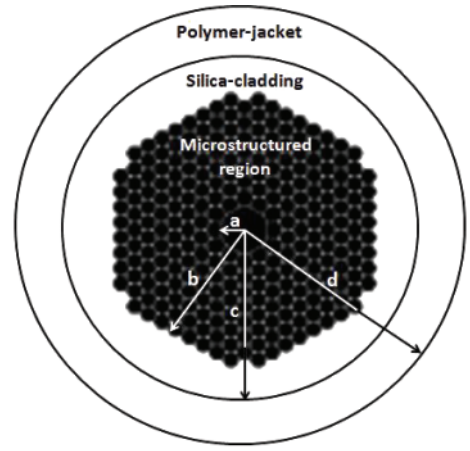

Figure 1: Cross-section of the investigated HC-PBF with an air-core, a microstructured air-silica inner cladding, a solid silica outer cladding, and a polymer coating, where (a–d) represent the radius of each region.

2. Mathematical Model

The cross-section of the investigated HC-PBF is shown in Figure 1. The HC-PBF is modeled as four circular regions, an air-core, an air-silica microstructured inner cladding consisting of array of cylindrical air holes, a solid silica outer cladding, and an acrylate layer. The parameters of each region of the HC-PBF are denoted by a superscript ($i = 1, 2, 3$, and 4). The HC-PBF is with 8 rings of arrays of air holes arranged in a triangular lattice with $\Lambda = 3.8\,\mu$m and $\eta = 92\%$. The air-core of diameter (d_1) is formed by removing seven central air holes.

The equations that describe the sound propagation in fluids are derived from the governing equations of fluid flow such as the mass conservation described by the continuity equation; the conservation of momentum, which is known as the Navier-Stokes equation; an energy conservation equation; the constitutive equations; and an equation of state that describes the relation between thermodynamic variables [13]. The acoustic pressure (p) is governed by the wave equation and is given by

$$\frac{1}{\rho_o c_o^2}\frac{\partial^2 p}{\partial t^2} + \nabla\cdot\left(-\frac{1}{\rho_o}\left(\nabla p - q\right)\right) = Q, \tag{1}$$

where t is the time, ρ_o is the density of the fluid, q and Q are the acoustic dipole and monopole source, respectively, and c_o is the velocity of the acoustic wave in the medium. The wave equation can be solved in the frequency domain to expand the acoustic signal into harmonic components via its Fourier series. A harmonic solution has the form

$$p(x, y) = p(x)\, e^{i\omega t}, \tag{2}$$

where ω is the angular frequency and the actual physical value of the acoustic pressure is the real part of (2); consequently, the time-dependent wave equation reduces to the Helmholtz equation given by

$$\nabla \cdot \left(-\frac{1}{\rho_o} \left(\nabla p - q \right) \right) - \frac{\omega^2}{\rho_o c_o^2} p = Q. \tag{3}$$

In the homogenous case where the two source terms q and Q are zero, the solution to the Helmholtz equation is the plane wave given by

$$p\left(x, y\right) = p_o\left(x\right) e^{i(\omega t - k \cdot x)}, \tag{4}$$

where p_o is the amplitude of the wave and it is moving in the k direction with angular frequency ω and wave number $k = |k|$. The acoustic pressure (p) acting on the microstructured fiber induces a stress distribution in the fiber's cross-section and structural deformation. Both factors affect the phase represented by a change in the fiber length and the effective refractive index and is given by

$$\varphi = \frac{2\pi}{\lambda} n_{\text{eff}} L, \tag{5}$$

where λ is the wavelength of the propagating light, and L is the length of the fiber. The applied acoustic pressure induces stress distribution in the optical fiber material. As a result of the stress-optic effect, stress induces anisotropic change of the index of refraction within the optical fiber. In this study, this process is achieved by coupling between the ASI and the EMW module in COMSOL Multiphysics. Acoustic pressures with different amplitudes and frequencies are applied by the ASI to obtain the induced strain and stress vectors and finally the index of refraction due to the stress-optic effect is calculated by the general linear stress-optical relation as follows [14, 15]. The general linear stress-optical relation is given by the tensor notation as

$$\Delta n_{ij} = -B_{ijkl} \sigma_{kl}, \tag{6}$$

where $\Delta n_{ij} = n_{ij} - n_o I_{ij}$, n_{ij} is the index of refraction tensor, n_o is the index of refraction for a stress-free material, I_{ij} is the identity tensor, B_{ijkl} is the stress-optical tensor, and σ_{kl} is the stress tensor. The number of independent parameters in the stress-optical tensor that characterizes this relation is reduced by symmetry. Because n_{ij} and σ_{kl} are both symmetric matrices, $B_{ijkl} = B_{jikl}$ and $B_{ijkl} = B_{ijlk}$. For the fiber material, the number of independent parameters is reduced to two independent parameters, $B_1 = -6.9 \times 10^{-13}$ m^2/N and $B_2 = -41.9 \times 10^{-13}$ m^2/N, that represent the first and second stress-optical coefficients, respectively [15]. In this case, the stress-optical relation simplifies to

$$\begin{bmatrix} \Delta n_x \\ \Delta n_y \\ \Delta n_z \end{bmatrix} = - \begin{bmatrix} B_1 & B_2 & B_2 \\ B_2 & B_1 & B_2 \\ B_2 & B_2 & B_1 \end{bmatrix} \begin{bmatrix} \sigma_x \\ \sigma_y \\ \sigma_z \end{bmatrix}, \tag{7}$$

where $n_x = n_{11}$, $n_y = n_{22}$, and $n_z = n_{33}$ are the refractive indices along the x-, y-, and z-axis, respectively, and $\sigma_x = \sigma_{11}$, $\sigma_y = \sigma_{22}$, and $\sigma_z = \sigma_{33}$ are the principal components of the induced stresses in the three directions. Using the two parameters B_1 and B_2, the model assumes that the nondiagonal parts of n_{ij} are negligible. As a result, the used general linear stress-optical relation, which describes the relation between the induced refractive indices and the principle stresses in x, y, and z directions, is reduced to

$$\begin{aligned} n_x &= n_o - B_1 \sigma_x - B_2 \left(\sigma_y + \sigma_z \right), \\ n_y &= n_o - B_1 \sigma_y - B_2 \left(\sigma_x + \sigma_z \right), \\ n_z &= n_o - B_1 \sigma_z - B_2 \left(\sigma_x + \sigma_y \right). \end{aligned} \tag{8}$$

For accurate calculations of modal characteristics of the investigated optical fiber, the full vectorial wave equations need to be solved. The FES COMSOL Multiphysics is used to solve the vectorial electric field wave equation as an eigenvalue problem and is given by [14, 16]

$$\nabla \times \left(\mu_r^{-1} \nabla \times E \right) - \lambda_e E = 0, \tag{9}$$

in which E is the electric field vector, μ_r is the relative permeability, and λ_e is the eigenvalue given by

$$\lambda_e = k_o^2 \varepsilon_r, \tag{10}$$

in which $k_o = 2\pi/\lambda$ is the free-space wave number and ε_r is the relative permittivity. In this model the electromagnetic wave, frequency domain interface, in the FES COMSOL Multiphysics is used for the mode analysis. The simulation is set up with the electric field components E_x, E_y, and E_z which are the dependent variables. The EMW can be described by the form [17]

$$\begin{aligned} E &= E\left(x, y\right) e^{j(-\alpha z)} \\ &= \left(E_x\left(x, y\right), E_y\left(x, y\right), E_z\left(x, y\right) \right) e^{j(-\alpha z)}, \end{aligned} \tag{11}$$

where the parameter $\alpha = \gamma + j\beta$ is the complex propagation constant, γ represents the attenuation along the propagation direction, and β is the propagation constant. The effective mode index of a confined mode is given by

$$n_{\text{eff}} = \frac{\beta}{k_o}. \tag{12}$$

The acoustic pressure primarily affects the L and n_{eff} terms in (5). The normalized responsivity (NR) is a figure of merit independent of wavelength and optical fiber dimensions are commonly used to compare between different hydrophone designs. NR of the HC-PBF is given by

$$\text{NR} = \frac{d\varphi}{\varphi\left(dp\right)} = \frac{1}{L}\frac{dL}{dp} + \frac{1}{n_{\text{eff}}}\frac{dn_{\text{eff}}}{dp} = \frac{\varepsilon_z^2}{dp} + \frac{1}{n_{\text{eff}}}\frac{dn_{\text{eff}}}{dp}, \tag{13}$$

where $\varepsilon_z^2 = dL/L$ is the axial strain of the microstructured region of the HC-PBF, and the superscript (2) is used to denote the microstructured region of the HC-PBF. In this paper, we are interested in calculating the index term of (13).

We investigate another area of research which is the effect of the acoustic pressure on the effective area A_{eff}, MFD, and NA of the HC-PBF. A_{eff} depends on fiber's index of refraction and the propagating wavelength, and accurate description of A_{eff} is based on ITU-T Petermann II definition and is given by [12, 17]

$$A_{\text{eff}} = \frac{\left[\iint_{-\infty}^{\infty} |E(x, y)|^2 \, dx \, dy\right]^2}{\iint_{-\infty}^{\infty} |E(x, y)|^4 \, dx \, dy}, \tag{14}$$

where $E(x, y)$ is the modal field distribution inside the fiber. A general relation between the MFD and A_{eff} is given by

$$A_{\text{eff}} = k(\lambda)\left(\frac{\pi}{4}\right)\text{MFD}^2, \tag{15}$$

where $k(\lambda)$ is wavelength dependent mapping value. If the electrical field distribution were Gaussian as in the case of conventional SMFs, the $k(\lambda)$ factor would be equal to one [11]. Furthermore, as d/Λ becomes larger, the correction factor $k(\lambda)$ approaches 1.2 for PCFs [11]. In this paper, $k(\lambda) = 1.2$ is considered.

The NA of the SC-PCFs is investigated in [18]. However, the calculation of NA in HC-PBF is different where the refractive index of the cladding is larger than that in the core [19]. A formula for the NA of HC-PBF was proposed in [11] and is given by

$$\text{NA} = \sqrt{1 - \left(\frac{\beta_U}{\beta_o}\right)^2}, \tag{16}$$

where β_U is the propagation constant of the upper edge of the bandgap and is related to the effective refractive index by $\beta_U = 2\pi n_{\text{eff}}/\lambda_U$, where λ_U is the wavelength corresponding to the upper edge of the bandgap. The NA of the PBF is wavelength dependent [11]. In this study, the effect of the acoustic pressure on the NA is calculated using (16) where the calculations are based on the calculated bandgaps of HC-1550 proposed in [7] and the propagation wavelength $\lambda_o = 1550$ nm and $\lambda_U = 1650$ nm.

As a conclusion, these calculations are performed by coupling between the ASI and the EMW frequency domain interface modules in the FES as follows: in the simulation setup of the EMW module, n_x, n_y, and n_z are inserted as the main diagonal elements of the anisotropic index of refraction tensor. Acoustic pressures with different amplitudes and frequencies that act on the investigated optical fiber are applied by the ASI. Once the induced stress distribution in the optical fiber is calculated, the anisotropic refractive index elements are calculated using (8), and the EMW module is used for mode analysis. Mode analysis study allows us to calculate n_{eff}, A_{eff}, MFD, and NA. By this way it is easy to obtain the relation between the applied acoustic pressure and the investigated parameters, and the contribution of the acoustic pressure induced n_{eff} change on φ and NR is calculated.

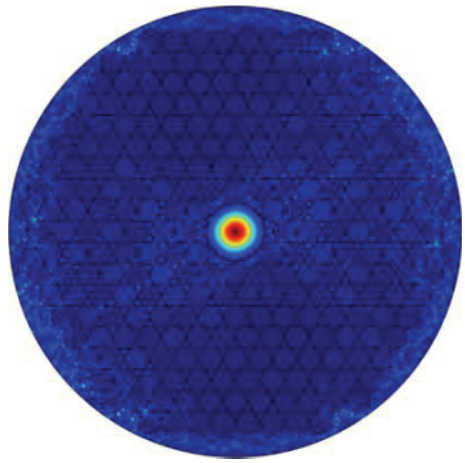

Figure 2: Fundamental mode confinement of the investigated optical fiber.

3. Simulation Results and Analysis

In this section, simulation results are introduced. The material's physical parameters of the investigated HC-PBF shown in Table 1 are imported into the FES. The microstructured region of the HC-PBF is modeled as anisotropic material while the silica outer cladding and the acrylate regions are modeled as isotropic materials [2]. The investigated HC-PBF is based on two-dimensional triangular structure with the air-core being formed by removing seven central holes. The index of refraction of silica cladding is 1.444, and the number of the air hole rings is eight. Perfectly matched layer (PML) is used to remove spurious reflections. We study the response of the HC-PBF to acoustic pressure by coupling between the ASI and the EMW modules in the FES. This allows easy transfer of the required data between the acoustics and electromagnetic waves modules and provides accurate calculations. After setting up the model geometry and inserting the required equations and data to the FES, the first step of calculations is to perform mode analysis for undeformed fiber. The calculated fundamental mode's intensity profile of the undeformed HC-PBF is shown in Figure 2, where $n_{\text{eff}} = 0.996128$. The second step is to use the acoustics module to apply acoustic pressure of different amplitudes and frequencies that cause structural deformation and the induced stresses and strains of the investigated fiber are calculated. The EMW module exchanges data with the ASI module by coupling between them and then by performing mode analysis; n_{eff} and A_{eff} corresponding to the deformed structure are calculated. This allows calculating the phase change and NR given by (5) and (13), respectively.

Figure 3 shows n_{eff} of the investigated HC-PBF as a function of the acoustic pressure at acoustic frequency 10 kHz. Due to applied acoustic pressure, the propagation constant changes because of two factors: the geometrical deformation and the change of the refractive index due to the stress-optic effect. From this figure, it can be seen that the calculated n_{eff} for the undeformed HC-PBF is 0.996128 and it increases as the acoustic pressure increases, where

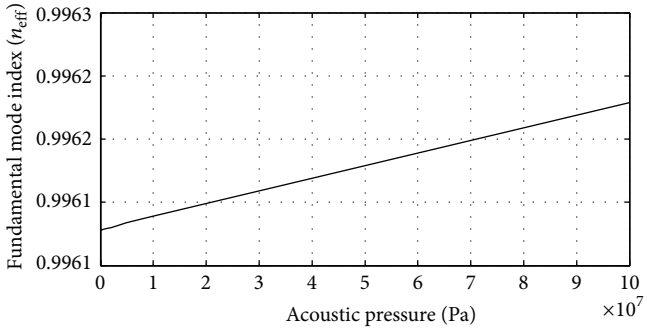

Figure 3: The calculated fundamental mode refractive index of the investigated HC-PBF as a function of the acoustic pressure at acoustic frequency 10 kHz.

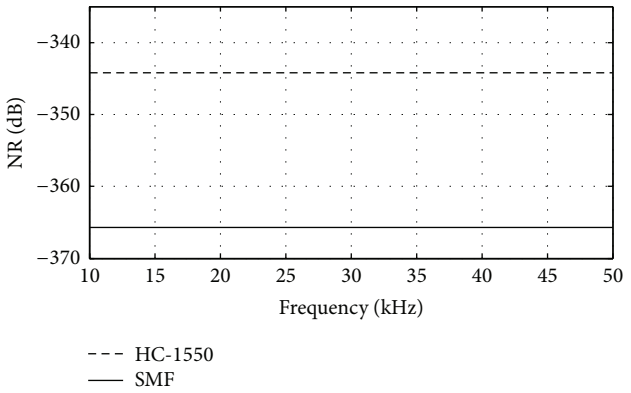

Figure 4: NR of the HC-1550 and SMF as a function of acoustic frequency.

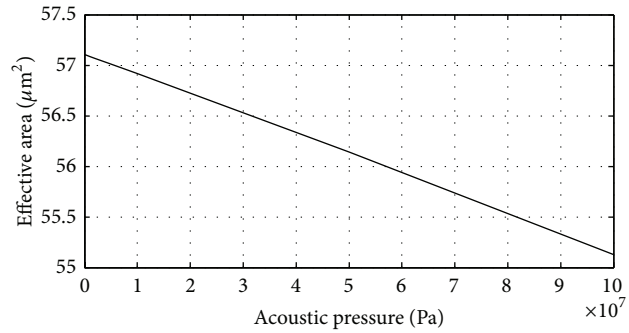

Figure 5: The calculated effective area of the investigated HC-PBF as a function of the acoustic pressure at acoustic frequency 10 kHz.

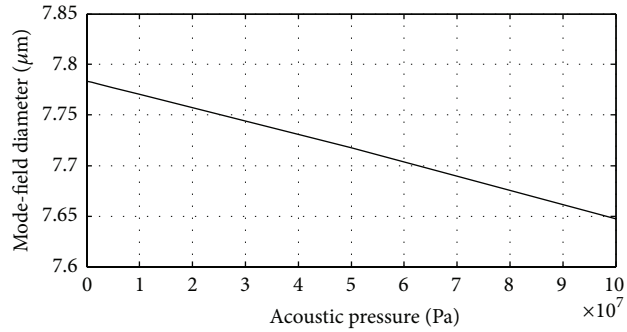

Figure 6: The calculated mode-field diameter of the investigated HC-PBF as a function of the acoustic pressure at acoustic frequency 10 kHz.

dn_{eff}/dp is 1.2×10^{-12} Pa^{-1}, where the acoustic pressure is swept from 0 to 100 MPa at frequency 10 kHz. Figure 4 shows the calculated NR of the HC-1550 and SMF as a function of acoustic frequency obtained from a previous study [20]. It can be seen that the calculated NR of the investigated HC-PBF is -2.5577×10^{-11} Pa^{-1}; consequently, from (13) the acoustic pressure-induced HC-PBF length change is -2.6777×10^{-11} Pa^{-1}. Simulation results showed that the contribution of the index change term to the total sensitivity of the HC-PBFs to acoustic pressure is minor with respect to the fiber length change. However, generally, for accurate design and simulations of the HC-PBFs, the index change term should be taken into account.

Figures 5 and 6 show the calculated effective area and MFD of the investigated HC-PBF as a function of the acoustic pressure at acoustic frequency 10 kHz. The calculated A_{eff} for undeformed fiber is 57.1 μm^2 while the MFD is 7.758×10^{-6} μm. It can be seen that the change in A_{eff} is inversely proportional to the acoustic pressure, where dA_{eff}/dp is -2×10^{-8} μm^2 Pa^{-1}, while the calculated MFD change with pressure is $d\text{MFD}/dp = -1.35 \times 10^{-15}$ μm Pa^{-1}.

Figure 7 shows the fundamental mode index corresponding to wavelengths 1550 nm and 1650 nm used to calculate NA of HC-PBF as a function of the acoustic pressure at acoustic frequency 10 kHz obtained by coupling the ASI and EMW modules in the FES, where the pressure is swept from 0 to 1 GPa. It can be seen that n_{eff} for the undeformed fiber of $\lambda = 1550$ nm and $\lambda = 1650$ nm is 0.996128 and 0.995313, respectively. Using (16) and the calculations proposed in this figure, we can preliminarily investigate the effect of acoustic pressure on the NA of the investigated HC-PBF. The calculated NA of the investigated HC-PBF as a function of the acoustic pressure at acoustic frequency 10 kHz is shown in Figure 8. It can be seen that NA for undeformed fiber is 0.3449383, and it is inversely proportional to the acoustic pressure where the change of NA with the acoustic pressure is $d\text{NA}/dp = -5.43 \times 10^{-13}$ Pa^{-1}.

4. Conclusion

In this paper, the FES COMSOL Multiphysics is used to study the effect of acoustic pressure on the fundamental mode of a HC-PBF, mainly on n_{eff}, A_{eff}, MFD, and NA. The proposed simulation results showed that the acoustic pressure-induced change of n_{eff} is 1.2×10^{-12} Pa^{-1}, where the acoustic pressure is swept from 0 to 100 MPa at frequency 10 kHz. Our previous study showed that the calculated NR of the investigated HC-PBF is -2.5577×10^{-11} Pa^{-1}; consequently, the acoustic pressure-induced HC-PBF length change is -2.6777×10^{-11} Pa^{-1}. It can be concluded that the contribution of the index change term to the total sensitivity of the HC-PBFs to acoustic pressure is minor with respect to the fiber length

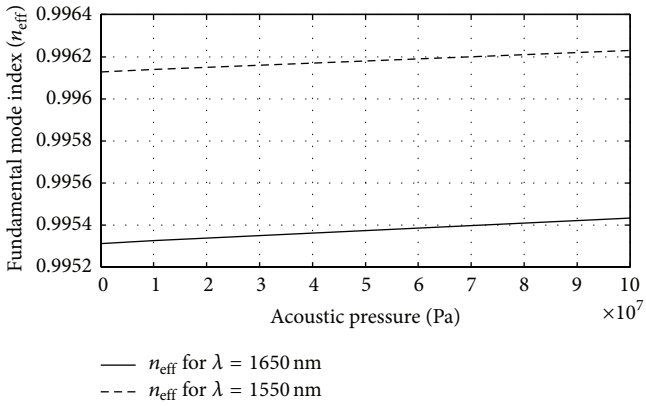

Figure 7: Fundamental mode index corresponding to wavelengths 1550 nm and 1650 nm as a function of the acoustic pressure at acoustic frequency 10 kHz.

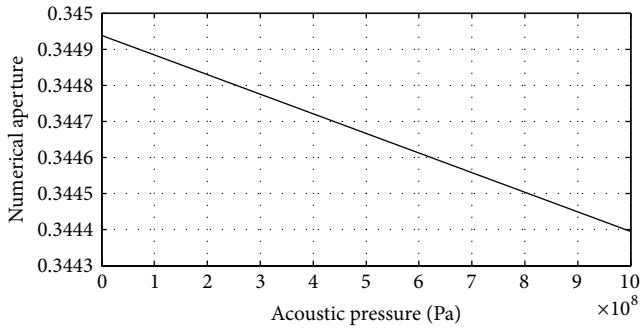

Figure 8: The calculated NA of the investigated HC-PBF as a function of the acoustic pressure at acoustic frequency 10 kHz.

change but it should be taken into account for accurate design and simulations of the HC-PBFs. Another area of research which is the effect of the acoustic pressure on the effective area A_{eff}, MFD, and NA of the HC-PBF is investigated. It is shown that the change in A_{eff} is inversely proportional to the pressure, where dA_{eff}/dp is $-2 \times 10^{-8}\ \mu\text{m}^2\ \text{Pa}^{-1}$, while the calculated MFD change with pressure is $d\text{MFD}/dp = -1.35 \times 10^{-15}\ \mu\text{m Pa}^{-1}$. Finally, we preliminarily investigated the effect of acoustic pressure on the NA of the investigated HC-PBF. It is shown that NA for undeformed fiber is 0.3449383, and it is inversely proportional to the acoustic pressure, where the change of NA with the acoustic pressure is $d\text{NA}/dp = -5.43 \times 10^{-13}\ \text{Pa}^{-1}$.

Conflict of Interests

The authors declare that there is no conflict of interests regarding the publication of this paper.

Acknowledgments

This work is supported by National Natural Science Foundation of China (61102004) and Fundamental Research Funds for the Central Universities.

References

[1] G. A. Cranch, P. J. Nash, and C. K. Kirkendall, "Large-scale remotely interrogated arrays of fiber-optic interferometric sensors for underwater acoustic applications," *IEEE Sensors Journal*, vol. 3, no. 1, pp. 19–30, 2003.

[2] M. Pang and W. Jin, "Detection of acoustic pressure with hollow-core photonic bandgap fiber," *Optics Express*, vol. 17, no. 13, pp. 11088–11097, 2009.

[3] Y. Léguillon, P. Besnard, L. Provino et al., "Phase sensitivity to axial strain of microstrustured optical silica fibers," in *21st International Conference on Optical Fiber Sensors*, vol. 7753 of *Proceedings of SPIE*, Ottawa, Canada, May 2011.

[4] M. D. Nielsen, J. R. Folkenberg, N. A. Mortensen, and A. Bjarklev, "Bandwidth comparison of photonic crystal fibers and conventional single-mode fibers," *Optics Express*, vol. 12, no. 3, pp. 430–435, 2004.

[5] H. K. Kim, M. J. F. Digonnet, and G. S. Kino, "Air-core photonic-bandgap fiber-optic gyroscope," *Journal of Lightwave Technology*, vol. 24, no. 8, pp. 3169–3174, 2006.

[6] NKT Photonics Website, 2013, http://www.nktphotonics.com/hollowcorefibers.

[7] W. Jin, H. F. Xuan, and H. L. Ho, "Sensing with hollow-core photonic bandgap fibers," *Measurement Science and Technology*, vol. 21, no. 9, Article ID 094014, 2010.

[8] F. Yang, W. Jin, H. L. Ho et al., "Enhancement of acoustic sensitivity of hollow-core photonic bandgap fibers," *Optics Express*, vol. 21, no. 13, pp. 15514–15521, 2013.

[9] H. Ademgil and S. Haxha, "Bending insensitive large mode area photonic crystal fiber," *Optik*, vol. 122, no. 21, pp. 1950–1956, 2011.

[10] N. A. Mortensen, "Effective area of photonic crystal fibers," *Optics Express*, vol. 10, no. 7, pp. 341–348, 2002.

[11] M. J. F. Digonnet, H. K. Kim, G. S. Kino, and S. Fan, "Understanding air-core photonic-bandgap fibers: analogy to conventional fibers," *Journal of Lightwave Technology*, vol. 23, no. 12, pp. 4169–4177, 2005.

[12] K. Miyagi, Y. Namihira, S. M. A. Razzak, S. F. Kaijage, and F. Begum, "Measurements of mode field diameter and effective area of photonic crystal fibers by far-field scanning technique," *Optical Review*, vol. 17, no. 4, pp. 388–392, 2010.

[13] COMSOL Multiphysics, *Introduction to the Acoustics Module*, 2013.

[14] COMSOL Multiphysics, *Wave Optics Module User's Guide*, COMSOL Multiphysics, 2013.

[15] M. Szpulak, T. Martynkien, and W. Urbanczyk, "Effects of hydrostatic pressure on phase and group modal birefringence in microstructured holey fibers," *Applied Optics*, vol. 43, no. 24, pp. 4739–4744, 2004.

[16] M. Koshiba and K. Saitoh, "Structural dependence of effective area and mode field diameter for holey fibers," *Optics Express*, vol. 11, no. 15, pp. 1746–1756, 2003.

[17] K. Saitoh and M. Koshiba, "Leakage loss and group velocity dispersion in air-core photonic bandgap fibers," *Optics Express*, vol. 11, no. 23, pp. 3100–3109, 2003.

[18] N. A. Mortensen, J. R. Folken, P. M. W. Skovgaard, and J. Broeng, "Numerical aperture of single-mode photonic crystal fibers," *IEEE Photonics Technology Letters*, vol. 14, no. 8, pp. 1094–1096, 2002.

[19] X. B. Xu, F. Y. Gao, Z. H. Zhang, J. Jin, and N. F. Song, "An investigation of numerical aperture of air-core photonic bandgap fiber," *Science China Technological Sciences*, vol. 58, no. 2, pp. 352–356, 2015.

[20] A. Abdallah, Z. Chaozhu, and Z. Zhi, "Phase sensitivity to acoustic pressure of microstrustured optical fibers: a comparison study," *International Journal of Signal Processing, Image Processing and Pattern Recognition*, vol. 8, no. 2, pp. 105–114, 2015.